SIRM 2019 – 13th International Conference on Dynamics of Rotating Machines,
Copenhagen, Denmark, 13th – 15th February 2019

Control Analysis of Wind Turbine Blade Vibration With SMA Actuators in Thermal Equilibrium

Rodrigo Nicoletti [1], **Robert Liebich** [2]

[1] São Carlos School of Engineering, University of São Paulo, 13566-590, São Carlos, Brazil, rnicolet@sc.usp.br
[2] Institut für Maschinenkonstruktion und Systemtechnik, Technische Universität Berlin, 10623, Berlin, Germany, robert.liebich@tu-berlin.de

Abstract

In this work, shape memory alloy (SMA) actuators are applied to wind turbine blades, aiming at reducing blade vibrations during operation. The work is focused on the application of SMA wires in thermal equilibrium on a 5 MW wind turbine blade (61.5 m long). The frequency response function of the SMA wire is modeled considering the thermal conditions of the blade and the constitutive law of the SMA material. This function is included in the state space model of the blade and a PD controller is designed by root locus analysis. The SMA wire geometry is found according to the maximum possible power output in the wind turbine blade. The numerical results show that this strategy is not feasible because the actuation force of the SMA is too small to make a significant effect on the blade dynamics. The necessary number of SMA wires to dynamically affect the blade is impractical.

Nomenclature

A_s	austenite temperature transformation	$\mathcal{P}$	SMA wire dissipated power
A_S	SMA wire cross section area	R_S	SMA wire radius
C_S	SMA wire specific heat	S	SMA wire heat transfer surface area
d_S	SMA wire diameter	t	time
e_0	bias voltage	T_o	blade surface temperature
E_M	SMA wire Young modulus	T_S	SMA wire temperature
f_S	SMA wire axial force	T_∞	environment temperature
G_P, G_D	proportional and derivative gains	$\mathcal{V}$	SMA wire volume
$\mathbf{G}$	gyroscopic matrix of the blade model		
h	heat convection coefficient	Γ	SMA wire operating condition parameter
k	thermal conductivity of the blade material	ε	SMA wire normal strain
$\mathbf{K}$	stiffness matrix of the blade model	Θ	SMA wire thermal expansion coefficient
l_2	distance from SMA wire to environment	ρ_e	SMA wire electric resistivity
L_S	SMA wire length	ρ_S	SMA wire density
$\mathbf{M}$	inertia matrix of the blade model	σ	SMA wire normal stress
N_S	number of SMA wires (one side of blade)	ω	frequency

1 Introduction

Vibration problems are among the top five causes of blade failure in the field [1]. The main reasons of such problems are the excessive bending moments, which can cause interlaminar failure and delamination, and high tip deflection, which can make the blades hit the tower [2]. All these failures are due to flapwise motion of the blade, but edgewise vibration can also occur during turbine parking or idling by vortex generation [3], which can cause trailing edge buckling. Trailing edge buckling can also be caused by an excessive weight load on slender blades [4].

Considering these facts, it has been increasingly necessary to include some sort of control device (passive or active) in the blades to mitigate vibration. The simplest approach to reduce blade vibrations is to include a tuned mass damper (passive control device) in the blades. However, in most of the times, wind excitation presents no

dominant frequency and, therefore, a more robust approach shall be looked for. Hence, many different active control devices have been investigated to tackle this problem: jet actuators, trailing edge flaps, microtabs, resonant controllers, active tendons, and active tuned mass dampers, among others, all of them presenting successful results in mitigating blade vibrations. A review of the morphing concepts and materials for wind turbine blade applications can be found in [5].

In this context, a shape memory alloy (SMA) actuator can be used in both control conditions: passive or active. Shape memory alloy is the generic name given to alloys which exhibit the unusual property of a strain-memory which can occur either at constant temperature or on changes of temperature [6]. Active application of SMAs were originally employed in helicopter blades [7]. In this case, SMA wires were used to control tabs in the trailing edge of the blades, aiming at keeping the blades in the same track during operation, thus representing a static operation of the SMA (actuation bandwidth was not a problem). More recently, SMA wires were employed to change the geometry of airfoils [8]. In this case, two antagonistic wires work together to move the trailing edge of an airfoil with successful results but presenting an actuation frequency bandwidth of $\sim$0.5 Hz (quasi-static application).

As we see in the literature, the long-time accommodation periods of thermal systems jeopardize the active application of SMAs, thus resulting in low bandwidth actuators. A possible solution to this problem is the adoption of SMAs working in its elastic phase and subjected to variations in temperature that will expand and contract the material. The best results were obtained in [9] with two antagonistic actuators in a pull-push operating condition (frequency bandwidth of 30 Hz). In this work, the feasibility of such strategy is numerically studied in the case of a 61.5 m long wind turbine blade with SMA wires mounted on its outer layers. The frequency response function of the SMA wire is modeled considering the thermal conditions of the blade and the constitutive law of the SMA material. This function is included in the state space model of the blade and a PD controller is designed by root locus analysis. The SMA wire geometry is found according to the maximum possible power output in the wind turbine blade.

2 Model of the SMA Actuator in Thermal Equilibrium

One way of using the SMA as actuators is avoiding the transformation of phase from martensite to austenite, i.e. by working in temperatures below A_s. For that, the SMA will work in its elastic phase, but variations in temperature will extend or contract the SMA wire, thus allowing to act on the structure it is mounted on. In this case, better results are obtained when two antagonistic actuators act together, in a pull-push operating condition [9]. To avoid the long-time accommodation periods of thermal systems that jeopardize actuation bandwidth, a bias electric voltage (e_0) is applied to the antagonistic wires and they work in the thermal equilibrium.

In the present case, the antagonistic SMA wires will be mounted in the top and bottom panels of the wind turbine blade, as shown in Fig. 1. By applying a bias electric voltage e_0 to both SMA wires, such configuration will present the temperature distribution in thermal equilibrium shown in Fig.2.

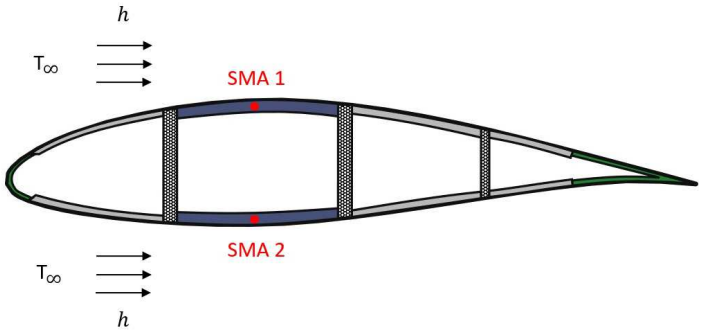

Figure 1: Cross section of the blade with the SMA wires in the top and in the bottom panels (flapwise direction).

Hence, the thermal equilibrium between the SMA wire and the surface of the blade is given by the heat dissipated by the electric voltage and the heat conducted to the blade surface:

$$-\frac{kS}{l_2}\left(T_S - T_o\right) + \frac{e_0^2}{R_S} = 0 \quad \Rightarrow \quad T_S = T_o + \frac{l_2 e_0^2}{kSR_S} \tag{1}$$

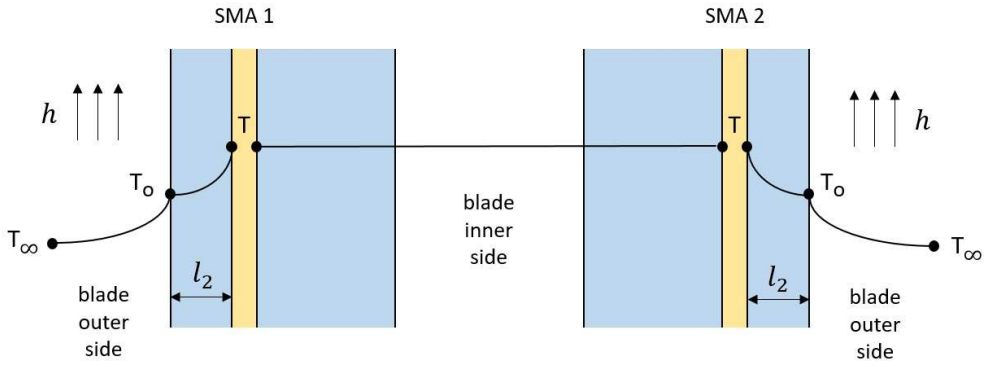

Figure 2: Thermal model of a wind turbine blade with embedded SMA wires in thermal equilibrium.

where S is the heat transfer area of the wire ($S = \pi d_S L_S/2$, half perimeter area).

In the surface of the blade, the heat conducted in the blade material is in equilibrium with the heat convection of the wind:

$$\frac{k}{l_2}\left(T_S - T_o\right) - h\left(T_o - T_\infty\right) = 0 \quad \Rightarrow \quad T_o = \frac{kT_S/l_2 + hT_\infty}{h + k/l_2} \tag{2}$$

Hence, from Eqs.(1) and (2) and considering that $S = \pi d_S L_S/2$ and $R_S = 4L_S\rho_e/\pi d_S^2$, then the temperature of the SMA wire in the thermal equilibrium is:

$$T_S = T_\infty + \left(\frac{l_2}{k} + \frac{1}{h}\right)\frac{d_S e_0^2}{2\rho_e L_S^2} < A_s \tag{3}$$

where ρ_e is the electrical resistivity of the SMA wire.

Hence:

$$\Gamma = \frac{d_s e_0^2}{L_S^2} < \frac{2\rho_e}{l_2/k + 1/h}\left(A_s - T_\infty\right) \tag{4}$$

where Γ is a parameter of the operating conditions of the SMA wire (function of the SMA wire diameter and length, and of the bias voltage).

The maximum admissible Γ increases by decreasing the thickness l_2 and the ambient temperature. Considering that higher Γ values allow the adoption of larger SMA wire diameters (d_S) and higher bias voltage (e_0), one can achieve higher force in the SMA actuator with such higher Γ values. Hence, one will adopt in the following analyzes the smallest thickness l_2 of 5 mm. Considering that the maximum admissible Γ value decreases with the ambient temperature, one will adopt in the following analyzes the ambient temperature of 15 ^{o}C, for safety reasons (if temperature decreases, the maximum admissible Γ increases).

Hence, considering the data in Table 1, the maximum admissible Γ_{max} value used in the following analysis will be 0.00265 V^2/m. Then, we can calculate the necessary length of the SMA wire as a function of its diameter and electric bias voltage:

$$\frac{d_S e_0^2}{L_S^2} \leq \Gamma_{max} \quad \Rightarrow \quad L_S \geq \sqrt{\frac{d_S e_0^2}{\Gamma_{max}}} \tag{5}$$

3 Actuator Frequency Response Function

When the pair of antagonistic actuators operate, an additional electric voltage is added to the bias electric voltage e_0. Therefore, the thermal equilibrium is disturbed and the temperature in the SMA wire changes, thus resulting in actuation forces. Hence, in the transient thermal regime, we have:

Table 1: Parameters used in the thermal equilibrium analysis of the blade with SMA wires.

parameter	value	unit
electric resistivity of the SMA wire (ρ_e)	80×10^{-8}	Ω.m
start temperature of austenite transformation (A_s)[1]	80	^{o}C
heat convection coefficient (h)	40	W/m^2.K
thermal conductivity of the blade material (k)	0.35	W/m.K

[1] high temperature SMA.

$$\rho_S C_S \frac{\partial T}{\partial t} = -\frac{kS}{l_2 \mathcal{V}} (T + T_S - T_o) + \frac{(e+e_0)^2}{R_S \mathcal{V}} \tag{6}$$

If $e \ll e_0$ and considering the equality of the thermal equilibrium in Eq.(1), then:

$$\rho_S C_S \frac{\partial T}{\partial t} = -\frac{kS}{l_2 \mathcal{V}} T + \frac{2e_0}{R_S \mathcal{V}} e \tag{7}$$

Considering that no phase transformation is expected in the SMA material and it will work in its elastic phase, the constitutive law of the SMA material [10] reduces to:

$$\sigma = E_M \varepsilon + \Theta T \quad \Rightarrow \quad T = \frac{f_S}{\Theta A_S} - \frac{E_M}{\Theta} \varepsilon \tag{8}$$

By inserting Eq.(8) into Eq.(7), we have:

$$\dot{f}_S + \frac{kS}{\rho_S C_S l_2 \mathcal{V}} f_S = A_S E_M \dot{\varepsilon} + \frac{A_S E_M k S}{\rho_S C_S l_2 \mathcal{V}} \varepsilon + \frac{2\Theta A_S\, e_0}{\rho_S C_S R_S \mathcal{V}}\, e \tag{9}$$

which in Laplace form gives:

$$F(j\omega) = A_S E_M E(j\omega) + \underbrace{\left(\frac{b_0}{j\omega + a_0}\right)}_{H(j\omega)} U(j\omega) \tag{10}$$

where:

$$a_0 = \frac{kS}{\rho_S C_S\, l_2 \mathcal{V}} = \frac{2k}{\rho_S C_S\, l_2\, d_S} \qquad \text{and} \qquad b_0 = \frac{2\Theta A_S\, e_0}{\rho_S C_S R_S \mathcal{V}} = \frac{\pi\, \Theta\, d_S^2\, e_0}{2\rho_S C_S \rho_e\, L_S^2} \tag{11}$$

for $A_S = \pi d_S^2/4$, $\mathcal{V} = \pi d_S^2 L_S/4$, $S = \pi d_S L_S/2$, and $R_S = 4\rho_e L_S/\pi d_S^2$.

As one can see in Eq.(10), the actuator force is proportional to the strain and it is a function of the electric voltage in the frequency domain. The amplitude of the force of the actuator in the frequency domain is given by:

$$|H(\omega)| = \frac{b_0}{\sqrt{\omega^2 + a_0^2}} = \frac{\pi\Theta\, l_2\, \Gamma_{max}\, d_S^2}{2\rho_e e_0 \sqrt{(\omega\, \rho_S C_S\, l_2\, d_S)^2 + 4k^2}} \approx \frac{\pi\Theta l_2 \Gamma_{max} d_S^2}{2\rho_e e_0\, \omega\, \rho_S C_S\, l_2\, d_S} \tag{12}$$

and the dissipated power in the actuator is given by:

$$\mathcal{P} = \frac{e_0^2}{R_S} = \frac{\pi d_S^2 e_0^2}{2\rho_e L_S} = \frac{\pi \Gamma_{max}^{1/2}\, e_0\, d_S^{3/2}}{4\rho_e} \tag{13}$$

Table 2: Parameters used in the calculation of the amplitude of actuator force and dissipated power.

parameter	value	unit
electric resistivity of the SMA wire (ρ_e)	80×10^{-8}	Ω.m
density of the SMA wire (nitinol) (ρ_S)	6,500	kg/m^3
specific heat of SMA wire (nitinol) (C_S)	836	J/kg.K
thermal expansion coefficient of the SMA material (Θ)	0.55	MN/m^2.K
maximum Γ value (Γ_{max})	0.00265	V^2/m
thermal conductivity of the blade material (k)	0.35	W/m.K
thickness of blade material (l_2)	5.0	mm
frequency of analysis (ω)	1.0	Hz

By calculating the amplitude of the actuator force at the frequency of 1 Hz (frequency near the first two natural frequencies of the wind turbine blade) and the respective dissipated power in the SMA wire, one obtained the results shown in Fig. 3 for different values of wire diameter and bias electric voltage using parameters listed in Table 2. As one can see, the actuator force increases with higher SMA wire diameters and lower bias electric voltages. The dissipated power in the SMA wire also decreases with lower electric bias voltage. Therefore, the bias electric voltage of $e_0 = 1$ V will be adopted in the following analysis. On the other hand, the dissipated power increases for higher SMA wire diameters, thus showing that higher forces require higher dissipated power in the SMA wires. The maximum actuator force achieved in the analysis ($|H|$ = 0.38 N/V @ 1 Hz) occurs for $d_S = 4.5$ mm, $e_0 = 1.0$ V, and L_S = 1.3 m. A response force of 0.38 N/V is rather small by taking into account that 15.3 W is dissipated in the SMA wire (a single wire).

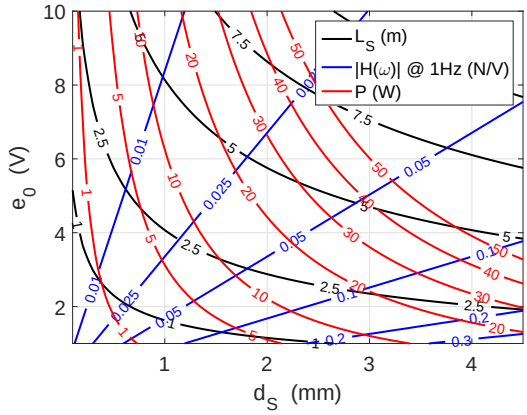

Figure 3: Amplitude of the actuator force at the frequency of 1 Hz and the respective dissipated power in the SMA wire for different values of wire diameter and bias electric voltage.

4 Actuator Design for Maximum Power Output in the Wind Turbine Blade

The problem of mounting antagonistic SMA wires on a wind turbine blade is the dissipated power in the wires. As shown in Fig. 3, the maximum actuation force is obtained with the maximum power dissipation. Hence, one cannot use an infinite number of SMA wires on the blade otherwise the dissipated power would also tend to infinite. Considering that the nominal output power of the turbine is 5 MW, it is interesting to establish a limit to the dissipated power in the actuation system. In this work, one adopted the limit of 1% of the nominal output power of the wind turbine, i.e. a limit of 50 kW.

From Eq.(13), considering two antagonistic SMA wires and knowing that the maximum dissipated power ($\mathcal{P}_{max}$) is 50 kW, one can calculate the maximum number of SMA wires in each side of the blade (N_S) based on the number of actuators along the blade (N_A):

$$N_S = \frac{2\,\rho_e\,\mathcal{P}_{max}}{\pi\,N_A\,\Gamma_{max}^{1/2}\,e_0\,d_S^{3/2}} \tag{14}$$

The length of each SMA wires is given by Eq.(5).

The model described in [11] will be used to calculate the maximum tip displacement and the maximum bending angle of the blade, with no wind and no rotation. This is a finite element model of the 61.5 m long blade of the upwind reference turbine [12], considering flapwise translation, edgewise translation, axial translation, and torsion in every node of the model. The actuation forces and moments of the SMA wires on the blade are applied to the nodes of the model, considering that the stress in the SMA wires in the i-th node of the model is:

$$\sigma_i = E_M \varepsilon_i + \frac{\pi\,\Theta\,l_2\,e_0\,d_S^3}{4k\rho_e L_S^2}\,e_i \tag{15}$$

where $i = 1, 2, ..., N_A$, and one considered that $\omega = 0$ Hz (static case – see Eq.(12)).

The maximum control voltage e_i is 0.2 V, and the SMA wires are mounted 5 mm apart from the surface of the blade (l_2). Two different configurations of SMA actuators are tested: actuators distributed along the blade ($N_A = 12$, Fig. 4a) and actuators concentrated at the end of the blade ($N_A = 6$, Fig. 4b). Figure 5 presents the results as a function of the SMA wire diameter.

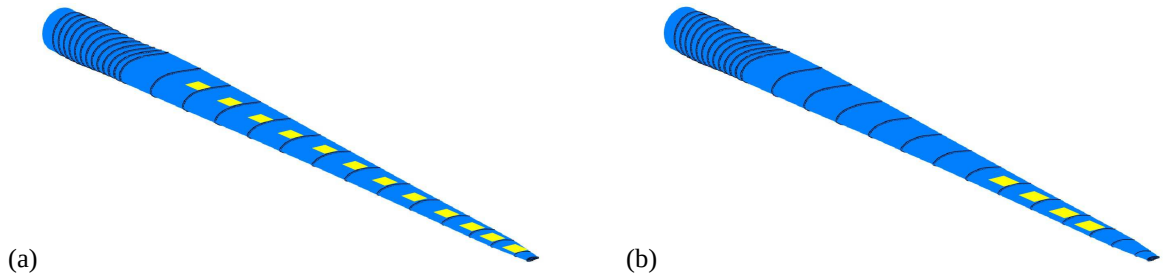

(a) (b)

Figure 4: Distribution of antagonistic SMA wires on the blade: (a) along the blade ($N_A = 12$); (b) at the end of the blade ($N_A = 4$).

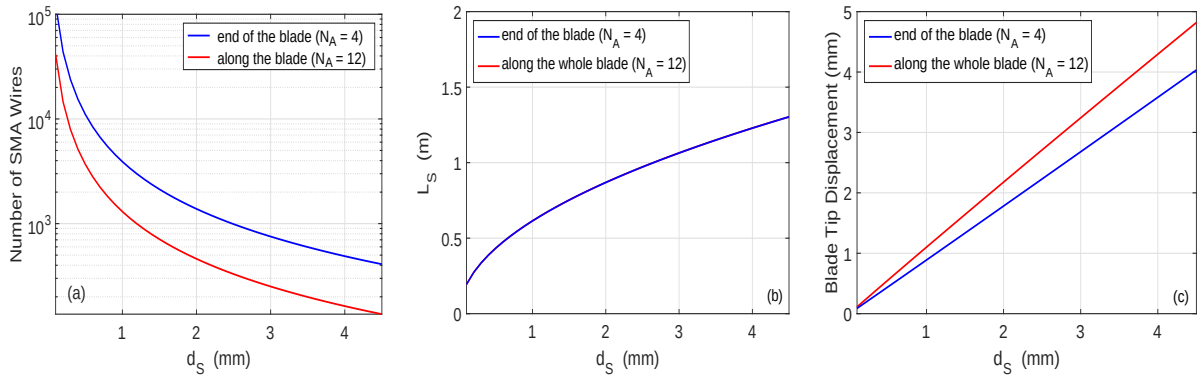

Figure 5: Maximum number of SMA wires, wire length, and maximum blade tip displacement as a function of the SMA wire diameter for a maximum dissipated power in the actuation system of 1% of the turbine output power (50 kW).

As we can see in Fig. 5, the maximum displacements of the blade occur for an SMA wire diameter of 4.5 mm. Better results are obtained by concentrating the actuators at the end of the blade, which is in accordance to previous results [11]. The length of the SMA wires does not depend on the distribution of SMA along the blade. Considering these results, the best set of parameters are: $N_A = 4$ (distribution on the blade), $N_S = 410$ (number of wires in each side of the blade), $d_S = 4.5$ mm (wire diameter), and $L_S = 1.3$ m (wire length).

It is important to emphasize that the above results are valid for static operation ($\omega = 0$ Hz). For dynamic operation, one has to analyze the system in closed loop feedback, considering the dynamics of the controller.

5 Closed-Loop Feedback and Root Locus Analysis

The equation of motion of the blade in Laplace form is:

$$\left(s^2\mathbf{M} + s\mathbf{G} + \mathbf{K}\right) X(s) = F_c(s) \tag{16}$$

where $X(s)$ is the vector of degrees-of-freedom of the blade model, and $F_c(s)$ is the vector of control forces.

The control forces come from the SMA wires, whose dynamics is described by Eq.(10), which in Laplace domain is:

$$F_c(s) = -\mathbf{B}A_S E_M \mathbf{C_1} X(s) - \mathbf{B}\left(\frac{b_0}{s+a_0}\right) U(s) \tag{17}$$

where the forces and moments are embedded in matrix $\mathbf{B}$, and we considered that there is a linear relationship between the strain and the degrees-of-freedom of the system embedded in matrix $\mathbf{C_1}$ ($E(s) = \mathbf{C_1} X(s)$).

The control voltage $U(s)$ comes from the chosen control law. In this work, we adopted a PD-control law, in the form:

$$U(s) = \left(G_P + sG_D\right) \mathbf{C_2} X(s) \tag{18}$$

where G_P and G_D are the proportional and derivative gains of the controller, respectively, and $\mathbf{C_2}$ is the observation matrix. Hence, we can write:

$$\begin{aligned}\left[s^2\left(s+a_0\right)\mathbf{M} + s\left(s+a_0\right)\mathbf{G} + \left(s+a_0\right)\mathbf{K} + \right.\\ \left.\left(s+a_0\right)\mathbf{B}A_S E_M \mathbf{C_1} + s\mathbf{B}b_0 G_D \mathbf{C_2} + \mathbf{B}b_0 G_P \mathbf{C_2}\right] X(s) = \mathbf{0}\end{aligned} \tag{19}$$

which gives:

$$\left[s^3\mathbf{A_3} + s^2\mathbf{A_2} + s\mathbf{A_1} + \mathbf{A_0}\right] X(s) = \mathbf{0} \tag{20}$$

where:

$$\begin{aligned} \mathbf{A_3} &= \mathbf{M} & \mathbf{A_1} &= a_0\,\mathbf{G} + \mathbf{K} + \mathbf{B}\,b_0\,G_D\,\mathbf{C_2} + \mathbf{B}A_S E_M \mathbf{C_1} \\ \mathbf{A_2} &= a_0\,\mathbf{M} + \mathbf{G} & \mathbf{A_0} &= a_0\,\mathbf{K} + a_0\,\mathbf{B}A_S E_M \mathbf{C_1} + \mathbf{B}\,b_0\,G_P \mathbf{C_2} \end{aligned} \tag{21}$$

From Eq.(20), we have:

$$\mathbf{A_3}\dddot{\mathbf{q}} + \mathbf{A_2}\ddot{\mathbf{q}} + \mathbf{A_1}\dot{\mathbf{q}} + \mathbf{A_0}\mathbf{q} = \mathbf{0} \tag{22}$$

or, in matrix form:

$$\underbrace{\begin{bmatrix} \mathbf{A_3} & & \\ & \mathbf{A_3} & \\ & & \mathbf{A_3} \end{bmatrix}}_{\mathbb{M}} \begin{Bmatrix} \dddot{\mathbf{q}} \\ \ddot{\mathbf{q}} \\ \dot{\mathbf{q}} \end{Bmatrix} + \underbrace{\begin{bmatrix} \mathbf{A_2} & \mathbf{A_1} & \mathbf{A_0} \\ -\mathbf{A_3} & & \\ & -\mathbf{A_3} & \end{bmatrix}}_{\mathbb{K}} \begin{Bmatrix} \ddot{\mathbf{q}} \\ \dot{\mathbf{q}} \\ \mathbf{q} \end{Bmatrix} = \begin{Bmatrix} \mathbf{0} \\ \mathbf{0} \\ \mathbf{0} \end{Bmatrix} \tag{23}$$

which gives the eigenvalue problem of the system with control feedback:

$$-\mathbb{K}Z = \mathbb{M}Z\lambda \tag{24}$$

where λ is the eigenvalue and Z is the eigenvector.

Considering that the eigenvalue problem of Eq.(24) is composed of matrices three times bigger than those of the mathematical model of the blade, it is interesting to perform a model reduction, in the form:

$$\mathbf{q} = \mathbf{\Phi}\eta \tag{25}$$

where $\mathbf{\Phi}$ is the reduced normal mode matrix composed of chosen eigenvectors, and η is the vector of modal coordinates.

Hence, the eigenvalue problem is reduced to:

$$-\mathbb{K}_r Z_r = \mathbb{M}_r Z_r \lambda \tag{26}$$

whose matrices are given by Eq.(23), but with the following coefficients:

$$\begin{array}{ll} \mathbf{A_3} = \mathbf{M}_r & \mathbf{A_1} = a_0\,\mathbf{G}_r + \mathbf{K}_r + \mathbf{E}_r + b_0\mathbf{G}_r^D \\ \mathbf{A_2} = a_0\,\mathbf{M}_r + \mathbf{G}_r & \mathbf{A_0} = a_0\,\mathbf{K}_r + a_0\,\mathbf{E}_r + b_0\mathbf{G}_r^P \end{array} \tag{27}$$

where:

$$\begin{array}{ll} \mathbf{M}_r = \mathbf{\Phi}^T\mathbf{M}\mathbf{\Phi} & \mathbf{E}_r = \mathbf{\Phi}^T\left(\mathbf{B}A_S E_M \mathbf{C_1}\right)\mathbf{\Phi} \\ \mathbf{G}_r = \mathbf{\Phi}^T\mathbf{G}\mathbf{\Phi} & \mathbf{G}_r^D = \mathbf{\Phi}^T\left(\mathbf{B}\,G_D\,\mathbf{C_2}\right)\mathbf{\Phi} \\ \mathbf{K}_r = \mathbf{\Phi}^T\mathbf{K}\mathbf{\Phi} & \mathbf{G}_r^P = \mathbf{\Phi}^T\left(\mathbf{B}\,G_P\mathbf{C_2}\right)\mathbf{\Phi} \end{array} \tag{28}$$

Equation (26) is used to calculate the eigenvalues of the system is closed loop to verify the effect of the SMA actuators in the dynamics of the blade. The reduced model of the blade considers the first ten normal modes listed in Table 3. Again, the blade is not subjected to wind and it does not rotate (same model used in the previous sections). A modal damping of 2% is added to the structure. The displacements and velocities of the nodes of the blade where the SMA wires are mounted are used as feedback parameters. The PD-controller gains are considered to be the same for all SMA actuators, and the derivative gain is scaled to be 5% of the proportional gain ($G_D = 0.05\,G_P$). The parameters of the SMA actuators are those listed in Table 2, which presented best performance in the static analysis. By solving the eigenvalue problem of Eq.(26) for different values of the proportional gain G_P, we obtained the results shown in Fig. 6.

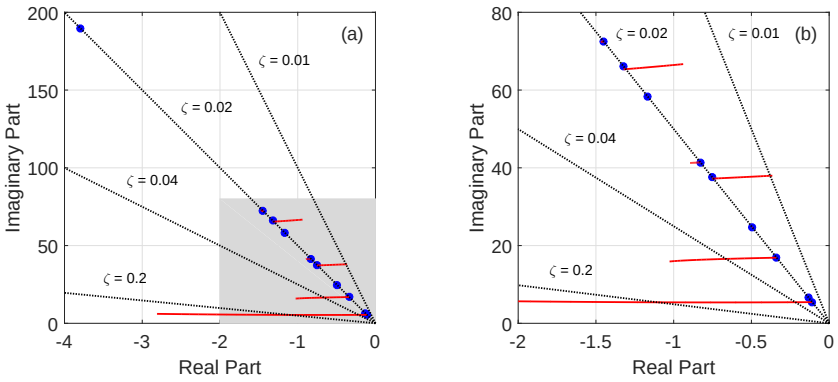

Figure 6: Loci of the eigenvalues of the blade model as a function of the proportional gain ($0 < G_P < 10^8$ V/m): (a) root loci; (b) zoom of shaded area.

Table 3: Normal modes considered in the reduced model of the blade.

mode	frequency (Hz)	type
1	0.868	1st. flapwise bending
2	1.044	1st. edgewise bending
3	2.702	2nd. flapwise bending
4	3.939	2nd. edgewise bending
5	5.987	3rd. flapwise bending
6	6.595	1st. torsion
7	9.284	3rd. edgewise bending
8	10.52	4th. flapwise bending
9	11.53	2nd. torsion
17	30.20	1st. axial

As we can see in Fig. 6, by increasing the proportional gain and, consequently, the derivative gain, the loci of the eigenvalues of the blade model move in the imaginary plane. The first and the third eigenvalues (associated to the first two bending modes in the flapwise direction) move towards higher damping regions. Such effect also happened to the sixth and to the ninth eigenvalues (associated to the first two torsion modes), but with small extent. On the other hand, the fifth and the eighth eigenvalues (associated to the third and fourth bending modes in the flapwise direction) move towards lower damping regions, thus showing that the system may become instable for higher gain values. The second, fourth, and seventh eigenvalues (associated to the first three bending modes in the edgewise direction) and the tenth eigenvalue (associated to the first axial mode) are not affected by the control system.

Hence, it is possible to change the eigenvalues of the blade by mounting the SMA actuators at its upper end. However, by looking at the necessary gain values to achieve such change, one can note that the application is not feasible. For example, the necessary proportional gain to double the amount of damping in the first bending mode of the blade ($\zeta = 0.04$, flapwise direction) is $3.3{\times}10^6$ N/V. It means that, if the blade moves 1 mm, the resultant control signal will be 3,300 V, which is much greater than the expected control signal e of 0.2 V from design. By limiting the control signal to 0.2 V, the maximum proportional gain would be 200 N/V (for a blade displacement of only 1 mm), and the resultant damping factor of the first bending mode in flapwise direction would be $\zeta = 0.020012$ (the same, for practical reasons).

6 Conclusion

This paper presents the mathematical modeling and the numerical analysis of the feedback control of a wind turbine blade with SMA wires working in thermal equilibrium. The results show that, the application of antagonistic SMA wires in a wind turbine blade is not feasible. Even adopting the best set of SMA parameters, the actuation force is too small to make any significant effect on the blade dynamics. In order to achieve a significant effect on the blade, it would be necessary a much higher number of SMA actuator and, consequently, much higher energy to operate. Considering that all the results presented here were obtained for a dissipated energy in the SMA actuators of 1% of the total output energy of the turbine, which is already a high value, a further increase in dissipated power would be impractical. And one must not forget that the turbine has three blades (all the previous analyses refer to a single blade).

Acknowledgment

This project was supported by Coordenação de Aperfeiçoamento de Pessoal de Nível Superior (Brazil) and by Alexander von Humboldt Stiftung (Germany) [grant number BEX 0190/15-2].

REFERENCES

[1] Chou, J.S., Chiu, C.K., Huang, I.K., Chi, K.N. (2013): Failure analysis of wind turbine blade under critical wind loads. *Engineering Failure Analysis*, **27**, pp.99-118.

[2] Branner, K., Ghadirian, A. (2014): *Database about blade faults.* DTU Wind Energy E-0067, Roskilde.

[3] Malkin, M., Griffin, D. (2016): *Edgewise vibration and wind turbine blade failure.* Available at www.windtech-international.com/editorial-features/edgewise-vibration-and-wind-turbine-blade-failure (accessed 9 August 2017).

[4] Jensen, F.M., Kling, A., Sørensen, J.D. (2017): *Change in failure type when wind turbine blades scale-up.* Available at energy.sandia.gov/wp-content//gallery/uploads/2B-A-1-Jensen1.pdf (assessed 9 August 2017).

[5] Lacehnal, X., Daynes, S., Weaver, P.M. (2013): Review of morphing concepts and materials for wind turbine blade applications. *Wind Energy*, **16**(2), pp.283-307.

[6] Worden, K., Bullough, W.A., Haywood, J. (2003): *Smart technologies.* Singapore: World Scientific Publishing.

[7] Kennedy, D.K., Straub, F.K., Schetky, L.M., Chaudhry, Z., Roznoy, R. (2004): Development of an SMA actuator for in-flight rotor blade tracking. *Journal of Intelligent Material Systems and Structures*, **15**(4), pp.235-248.

[8] Abreu, G.L.C.M., Maesta, M.F., Lopes, V.Jr., de Marqui, C.Jr., Faria, C.T., Inman, D.J. (2015): Active angular control of a sectioned airfoil using shape memory alloys and fuzzy controller. *Journal of the Brazilian Society of Mechanical Sciences and Engineering*, **37**(5), pp.1555-1567.

[9] Susuki, Y, Kagawa, Y. (2010): Active vibration control of a flexible cantilever beam using shape memory alloy actuators. *Smart Materials and Structures*, **19**(8), pp.085014.

[10] Brinson, L.C. (1993): One-dimensional constitutive behavior of shape memory alloys: thermodynamic derivation with non-constant material functions and redefined martensite internal value. *Journal of Intelligent Material Systems and Structures*, **4**(2), pp.229-242.

[11] Nicoletti, R., Liebich, R. (2018): Analysis of long wind turbine blades with shape memory alloy wires in super-elastic phase. *Journal of Intelligent Material Systems and Structures*, **29**(15), pp.3108-3123.

[12] Jonkman, J., Butterfield, S., Musial, W., Scott, G. (2009): *Definition of a 5-MW reference wind turbine for offshore system development*. National Renewable Energy Laboratory, Golden, Report NREL/TP-500-38060.